REMOVING MATERIAL NOISE IN EDDY-CURRENT INSPECTIONS OF STEAM GENERATORS TUBES USING WAVELET TRANSFORM

Luiz Antonio Negro Martin Lopez
The University Center of FEI, Mechanical Engineering Department
Av. Humberto A. C. Branco, 3972 – São Bernardo do Campo – SP – Brazil – 09850-901
tel# 55-11-43532900 r. 2172 – luizlope@fei.edu.br

Daniel Kao Sun Ting
Instituto de Pesquisas Energéticas e Nucleares, IPEN/CNEN-SP, Nuclear Engineering Center
Av. Prof. Lineu Prestes, 2242– Cidade Universitária, São Paulo – SP – Brazil – 05508-900
tel# 55-11-38169423 – dksting@net.ipen.br

Belle R. Upadhyaya
The University of Tennessee, Nuclear Engineering Department
Knoxville, TN 37996-2300
tel# +1-865-974-7576 – bupadhya@utk.edu

Abstract. *The signals generated during a Eddy Current Testing (ECT) inspection in steam generator tubes of both nuclear or conventional power plants allows for the localization and dimensioning of defects in the tubes. A noise free ECT signal has a "eight" shaped Lissajous figure in the impedance plane which main characteristics are the phase angle and amplitude. However, in the real practice, ECT signals are corrupted by several forms of noise, which can interfere in the analysis of the acquired signal, reducing the correct/misreading ratio and increasing the duration of the inspection.*
This present work presents a methodology to remove the noise caused by non-uniformities in the material being inspected, which we named as Material Noise. This noise is introduced by dimensional variations and non-homogeneities in the magnetic properties of the material, which can produce significant distortions in the Lissajous figure, inducing to misreading of the phase angle and amplitude. In some cases, the distortions are so serious that readings are not possible at all.
The methodology presented is based on processing the signal using Wavelet Transform, since the ECT signals are transient, producing ***Defect Codes,*** *which are composed by a set of selected coefficients of the transform used in the signal reconstruction. These* ***Defect Codes*** *can be used to establish a calibration procedure for each type of material, producing standardized Lissajous figures related to each known type of defect, constituting a* ***Defect Library****.*
The methodology was tested with signals obtained from inspections in experimental stainless steel tubes with implanted known defects and the results have demonstrated the applicability of the method.

Keywords: *De-noising, Eddy-Current Testing, Steam Generator, Wavelet Transform*

1. Introduction

Eddy Current Testing (*ECT*) for defects in heat exchangers tubes of a nuclear or conventional power plant is the most widely used and accepted technique for many years. The signals generated during an Eddy-Current Testing (*ECT*) in Steam Generators tubes (*SG*) contain noise, which can jeopardize the determination of the main signal characteristics such as the phase angle and the total amplitude. These characteristics allow for the detection, localization and sizing of the defects in and on the tube.

ECT signals have both the resistive (R) and the inductive (X_L) components and when they are presented in the complex plane, they have the form of a Lissajous figure with a typical "8" shaped curve when no noise is present, in an ideal setting. The phase angle and the total amplitude of a signal are read according to the definitions shown in Figure 1.

The phase angle is the angle formed by the straight line common to the two petals of the Lissajous figure and a horizontal line, measured counter clockwise. The total amplitude is the measurement in Volts between the two extreme points of the Lissajous figure petals (Stegemann, 1986).

The phase angle allows for the determination of the position of the defect either at the internal wall or at the external wall of the tube. The phase angle also allows for the determination of the defect depth by using the inspection instrument calibration curve, according to the Figure 2, which is standardized by the ASME Code, Section V, Article 8, Appendice 1. According to the calibration curve, a full depth defect presents a phase angle of 40^{o}.

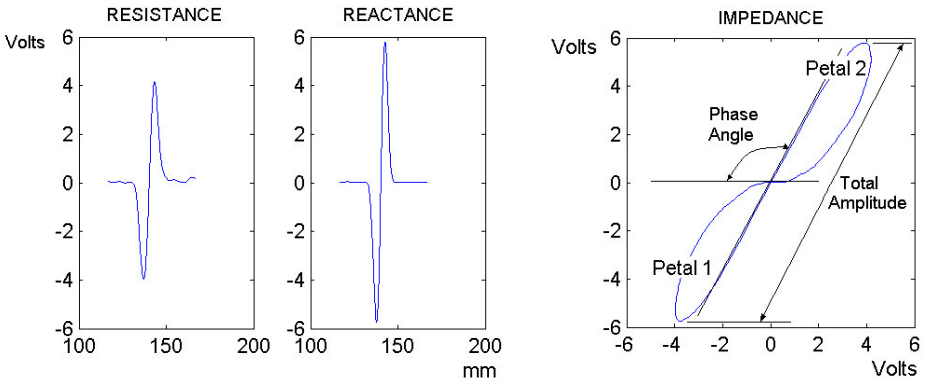

Figure 1. A typical noise free *ECT* signal and its characteristics

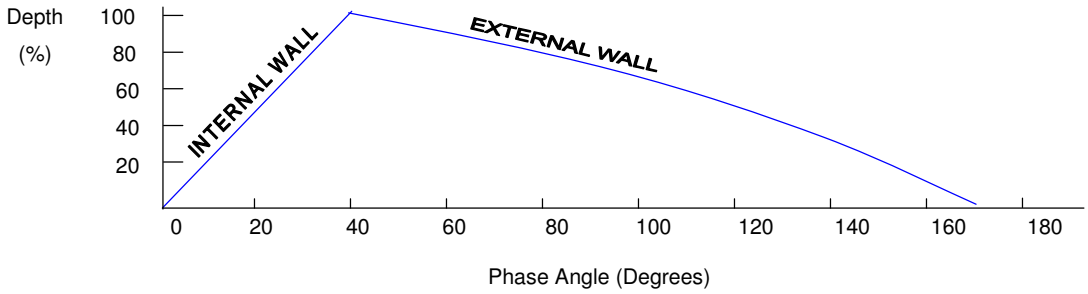

Figure 2. Typical *ECT* Instrument Calibration Curve

Actually, *ECT* signals acquired during an inspection contain noises, which can strongly interfere in their analysis (Upadhyaya, *et al*., 1995). These noises have many origins like those introduced by the data acquisition instrumentation (Lopez, *et al.*, 2003) or by the radial movement of the probe inside the tube. Two types of noise related to the material itself are: those caused by chemical deposits on the surface and those caused by non-homogeneities of the material itself. This present work focuses on the noise generated in the material itself, here named as Material Noise (*MTN*). The *MTN* is a noise originated in dimensional fluctuations and also, in the variations of the magnetic properties of the material, caused for example by the manufacturing process such as longitudinal welding in tubes. These noises can produce distortions in the Lissajous figures to such an extension, where phase angles and amplitudes readings are simply impossible at all. The Figure 3 presents a seriously affected *ECT* signal by *MTN*.

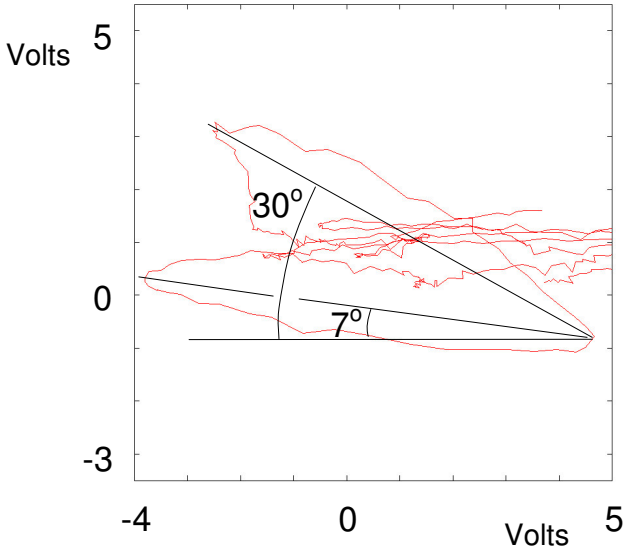

Figure 3. A typical *ECT* signal affected by Material Noise

When confronted by such a distorted *ECT* signal, the inspector has a dilemma and he should decide whether to consider a 7° phase angle characterizing a internal defect with about 15% wall thickness depth, or 30°, which represents a 70% wall thickness depth internal defect. The deviations are significant and produce a non conclusive testing, inducing the inspector to decide between a 15% or 70% wall thickness defect while the actual correct diagnosis should be a 100% full depth defect!

A methodology for the removal of *MTN* using Wavelet Transform (*WT*) is presented. Signals contaminated by *MTN* are processed using *WT* generating noise free Lissajous figures compatible with the known defects. To illustrate the methodology applicability, signals generated by the Zetec MIZ 17-ET with circumferential probes in stainless steel tubes with longitudinal welding, ASTM A-249-316L, ∅ 19,05 mm, 1,24 mm wall thickness (BWG 18) with full penetration defects artificially produced using electro erosion on the longitudinal welding.

2. The Wavelet Transform

The Wavelet Transform (*WT*) was first proposed by Mallat (1989). This type of time-scale signal transformation combines the use of variable time windows and variable scales, allowing the use of large time intervals when precise lower frequency information is needed as well as smaller time intervals when high frequency information is required.

A *WT* is very sensitive to discontinuities in the time domain, which is typical of *ECT* signals. It is a method where the transformed time frequency domain can be varied, in other words, the resolution of the time frequency domain is not constant, allowing for a more detailed description of the time frequency behavior of the signal being analyzed. Using this tool, one can analyze the signal in as many separated frequency bands as needed.

In this transform, the set of sub-spaces $\{V_j\}_{j \in Z}$ is a multi-resolution approximation of $L^2(R)$ if it contains a series of particular properties, where Z is a set of integrals. These particular properties establish that $\{V_j\}_{j \in Z}$ is associated to a sequence of sub-spaces, which covers the domain $L^2(R)$. In other words, if any square of the modulus of a given function has a well defined integral then it can be approximated with the necessary precision by a function that is inside of at least one of the sub-spaces V_j. Therefore, the functions which represent a *WT*, that have its modulus squared integrated in the real domain, can be represented by the condition:

$$\int_{-\infty}^{+\infty} |f(x)|^2 dx < \infty \tag{1}$$

The sets of functions that are generated by a *WT* are obtained by expansion (scale changes) and by translation (time shifts) of a simple prototype function $\psi(x)$, called the Wavelet function. This function is time dependent and generally centered, decaying rapidly as $|x| \to \infty$. The Wavelet function is a waveform with a total length that is limited by the scale, being more expanded or compressed depending of the chosen scale.

A basic Wavelet function $\psi(x) \in L^2(R)$ has two characteristic parameters, named : the scale '*a*' and the position '*b*', which change continually. A complete set of basic Wavelet functions $\psi_{a,b}(x)$ can be obtained by the dilation and shifting of $\psi(x)$ according to:

$$\psi_{a,b}(x) = \frac{1}{\sqrt{|a|}} \psi\left(\frac{x-b}{a}\right) \tag{2}$$

Where $(a,b) \in R$ and $a \neq 0$

For a given *ECT* signal $s(x)$, the *WT* is the convolution of $s(x)$ with a set of Wavelet functions $\psi_{a,b}(x)$ resulting in a set of coefficients $C_{a,b}$ as follows:

$$C_{(a,b)} = \int_{-\infty}^{+\infty} s(x)\ \psi_{a,b}(x)\, dx \tag{3}$$

If one multiplies each coefficient by the properly dilated and shifted Wavelet function one should regenerate the original function $S(x)$. There exists a relationship between the Wavelet scale and the frequency, in other words, a small scale will produce a compressed Wavelet where the details change rapidly in higher frequencies (ω), while with a large scale, the Wavelet is expanded and details change slowly with lower frequencies (ω).

3. Methodology

Processing *ECT* signals to remove *MTN* is performed by transforming the data to the time frequency domain using multiple scale levels by a Wavelet transform. A given signal $S(x)$ is decomposed in each scale level into a approximation component A_i and a detail D_i , according to the decomposition tree shown in Figure 4.

The approximation A_i at a given level i is the high scale component at that level containing the low frequency information. In the other hand, the detail D_i is the low scale component with the high frequency content. Each

approximation A_i is decomposed by its turn in another approximation and detail successively. For ***n*** level decompositions, there exists ***n+1*** possible decompositions for a given signal.

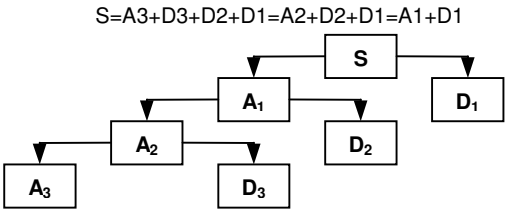

Figure 4. Multiple level *WT* decomposition tree.

The processing of the signal in a computer can be made more efficient if one uses the Discreet Wavelet Transform (*DWT*) based on dyadic scales. After decomposing the signal in multiple levels the *MTN* is removed by a process known as denoising. The *MTN* is a low frequency component noise with large amplitudes, which can be removed by selecting a proper combination of the coefficients $C_{a,b}$ to denoise. This set of coefficients $C_{a,b}$ representing the noise content will be named the *DEFECT CODE* and it will be characterized for each type of most commonly known defects.

The removing of *MTN* is performed separately for the resistive and inductive parts of the signal for a given defect. The *MTN* is much more visible in the resistive part of the signal which is more affected by geometrical fluctuations as well as by magnetic properties non-homogeneities. After denoising, the signal is recovered without the *MTN* generating afterwards a Lissajous figure compatible with the defect sought, i.e., it has a "8" shape form and presents a readable phase angle and amplitude values.

The result of this procedure is the determination of the set of *WT* coefficients, which does the best *MTN* removal, generating the associated *DEFECT CODE* for that defect. The codes associated to these coefficients $C_{a,b}$ are related to the type of material of the tubes, the type of *MTN*, the tube manufacturing specification, and can therefore be added and constituting a *DEFECT LIBRARY*. These defect codes can then be used in similar tubes inspections.

During an actual inspection, the measuring instrument must be calibrated. The removal of *MTN* can be considered as part of calibration procedure when the set of *DEFECT CODE* can be determined and the signals will be denoised previously, before the analysis itself. Some examples of *MTN* removal from *ECT* signals and the determination of the correspondent defect codes will be shown below.

3.1 Applying the methodology – An example

Figure 5 presents the signal of a full depth hole with ∅ 0,9 mm and the phase angle cannot be read due to strong *MTN* contamination, resulting in a Lissajous figure that is far from a "8" shaped figure. Since it is a full depth hole it is known that the phase angle should be 40°. The total amplitude for the inductive component reading is 4,4 V. The *MTN* can be seen in the region between –1V and 5V in the horizontal scale and between 0V and 1.5V in the vertical scale. For an inspector, this signal reading is not reliable and would not lead to a conclusive diagnostics.

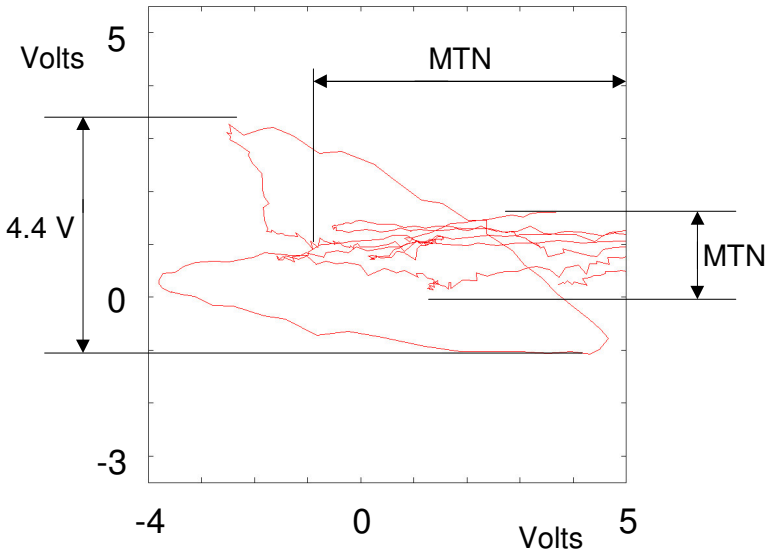

Figure 5. Lissajous figure for a ∅ 0,9 mm full depth hole

The first step is to separate the resistive component (R) and the inductive component (X_L) of the ECT signal as it is shown in Figure 6.

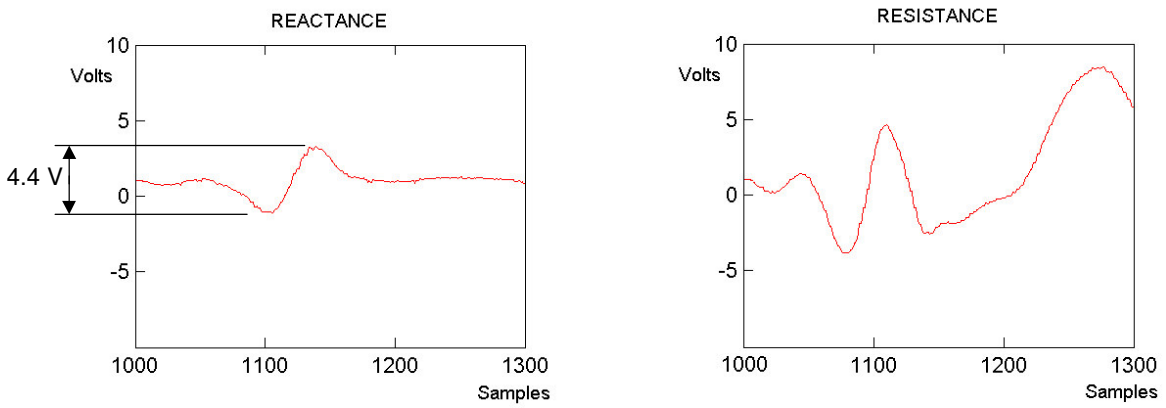

Figure 6. Resistive and inductive components for a ∅ 0,9 mm full depth hole

Comparing above signal with the ideal condition (Figure 1) one can notice that the Lissajous figure distortion is caused by noise in the resistive component contribution, which is much more significant than those in the inductive component. The signal to noise ratio for the resistive component is always above unity while the inductive component ratio is less than unity.

The tube was manufactured with a longitudinal welding. The external diameter is 19,05 mm ± 0,10 mm. The wall thickness is 1,24 mm ± 0,10 mm. The large fluctuation in the wall thickness associated to magnetic changes caused by the welding process produced significant *MTN*.

The full depth hole with ∅ 0,9 mm defect signal was processed using several different types of Wavelets. Figure 7 presents the results obtained using a Daubechies 5 with 8 scale levels. From the resistive component the approximation A8 and the details D1 a D5, 11/13 D6, D7 e D8 were removed. From the inductive component the details D1 a D3 were removed. In this way, 2/3 of the detail D6 for the resistive component and the details D4 and D8 as well as the approximation A8 for the inductive component remained. The recovered signal will be:
$S=(2/13D6)_R+ (A8+D8+D7+D6+D5+D4)_{XL}$.

The corresponding *DEFECT CODE* will be named: Db5L8R2/13D6XLD4-D8A8.

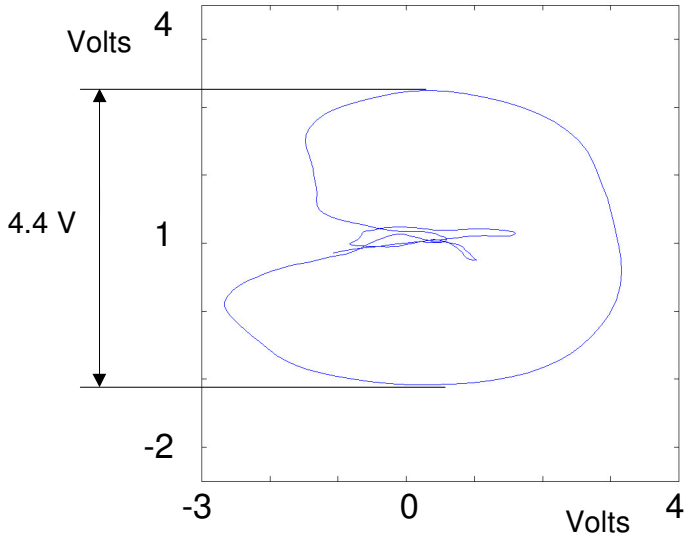

Figure 7. First denoised signal (full depth hole ∅ 0,9 mm)
DEFECT CODE: Db5L8R2/13D6XLD4-D8A8

One can observe in Figure 7 that the inductive voltage range is kept the same as the original value and that although the shape resembles a "8" form without edges, no center or a crossing point between the two petals is present. Without this crossing point and the two petals, it is not possible to determine the phase angle of an *ECT* signal.

In Figure 8 the same signal is denoised with a Daubechies 5 Wavelet. But this time with a different set of coefficients: in the resistive component, approximation A8 and details D1 to D3 and D6 to D8 were removed while in the inductive component, details D1 to D3 were removed. In this way, the recovered signal will be:
$S= (D5+D4)_R + (A8+D8+D7+D6+D5+D4)_{XL}$.

The corresponding *DEFECT CODE* will be named Db5L8RD4D5XLD4-D8A8.

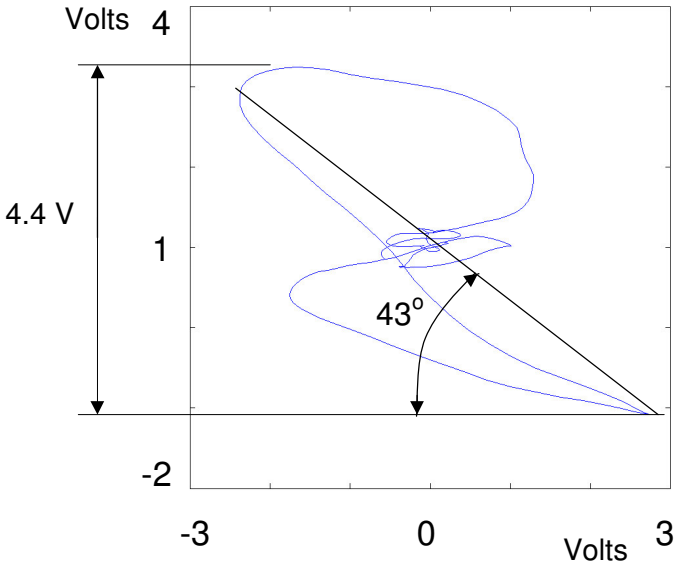

Figure 8. Second denoised signal (full depth hole ∅ 0,9 mm)
DEFECT CODE: Db5L8RD4D5XLD4-D8A8

This second denoised signal presents a better result compared to the first one, since it presents a central crossing point between two petals and it is possible to determine a phase angle of 43°. However, the lower petal is sharp edged and is not symmetrical when compared to the upper petal. The symmetry is expected characteristic when compared with a standard "8" shape figure for a full depth through hole defect.

A third set of *WT* coefficients were determined, imposing again that the voltage range in the inductive component to be kept the same. This third denoised signal is presented in figure 9, where a much better "8" shape figure was obtained and the measured phase angle is 39°, which is closer to the standard value of 40°. In this case, the same Daubechies 5 Wavelet with 8 scale levels was used, removing the lower inductive frequencies (D1 to D4 and 16/18 D5) and details D1 to D4, 16/18/D5 to D6 a D8, approximation A8 from the resistive part was removed.

The recovered signal will therefore be $S=(2/18D5)_R+(A8+D8+D7+D6+4/18D5)_{XL}$, and the *DEFECT CODE* is Db5L8R2/18D5XL4/18D5D6-D8A8.

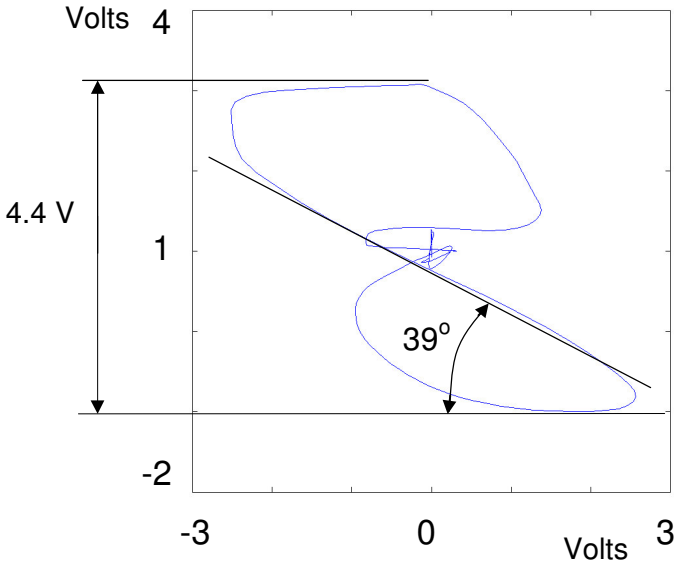

Figure 9. Third denoised signal (full depth hole ∅ 0,9 mm)
DEFECT CODE: Db5L8R2/18D5XL4/18D5D6-D8A8

Finally, a better denoising is presented in Figure 10 where a Lissajous figure very similar to the last one were obtained using the same code for the resistive component (R2/18 D5). From the inductive component, however, the two lowest frequency band D1 and D2 were removed. The recovered signal will be:

$S= (2/18D5)_R + (A8+D8+D7+D6+D5+D4+D3)_{XL}$.

The resulting *DEFECT CODE* will therefore be Db5L8R2/18D5XLD3-D8A8. By keeping the frequency bands from D3 and up, distorted the lower petal but reduced the dimensions thus improving the symmetry between the two petals which is desirable when comparing with the standard "8" shape figure for this type of defect. The measured phase angle is 38° which is also close to the standard value of 40° and the voltage range were kept the same as the original values which is a important criteria to be satisfied since original resistive amplitudes are kept constant.

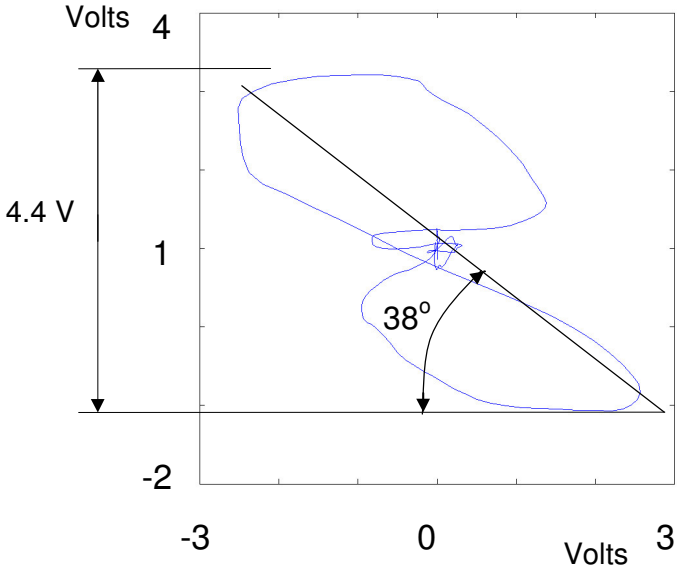

Figure 10. Final denoised signal (full depth hole ∅ 0,9 mm)
DEFECT CODE: Db5L8R2/18D5XLD3-D8A8

Figure 11 presents the original signal in red color and the final denoised signal in blue color.

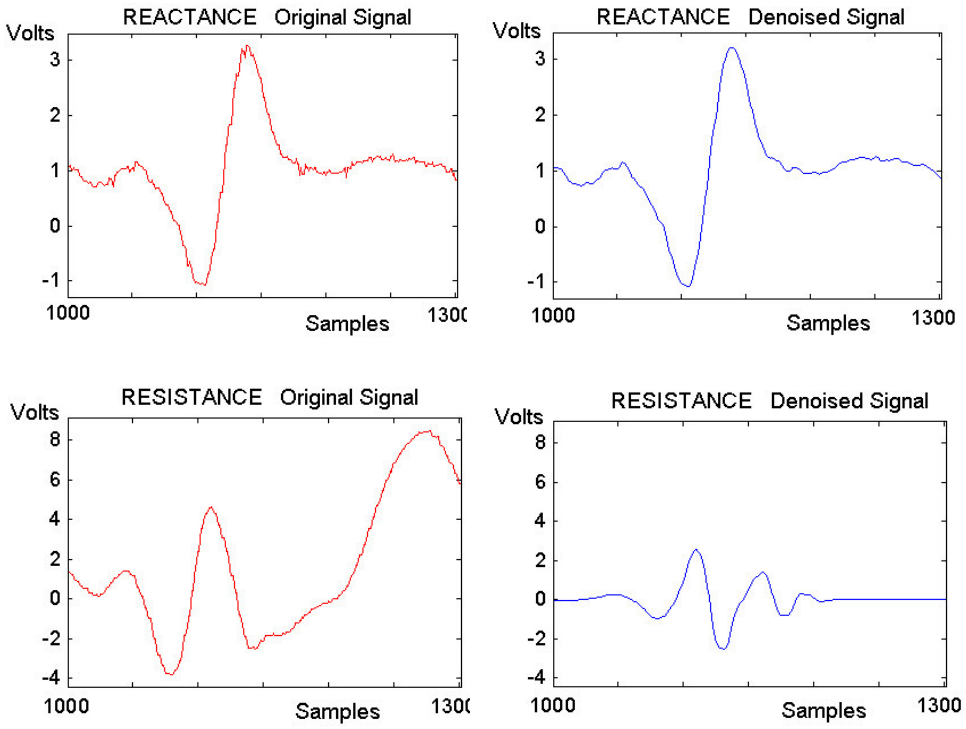

Figure 11. Original and denoised resistive and inductive components for a ∅ 0,9 mm full depth hole

4. Discussion about this methodology

Although the above described methodology presented good results as shown above, we found out that when the same *DEFECT CODE* is applied to another defect, with the same characteristic in the same tube, the shape of the Lissajous figure improved significantly but the denoising was less efficient. As an example, if the code Db5L8R2/18D5XLD3-D8A8, obtained for the ∅ 0,9 mm defect is used in a ∅ 1,1 mm defect in the same tube, also produced by electro erosion on the welding, the original Lissajous figure which is totally distorted (Figure 12a) evolves satisfactorily in just one step denoising to a "8" shaped figure (Figure 12b). However, the petals are not symmetrical as they should be.

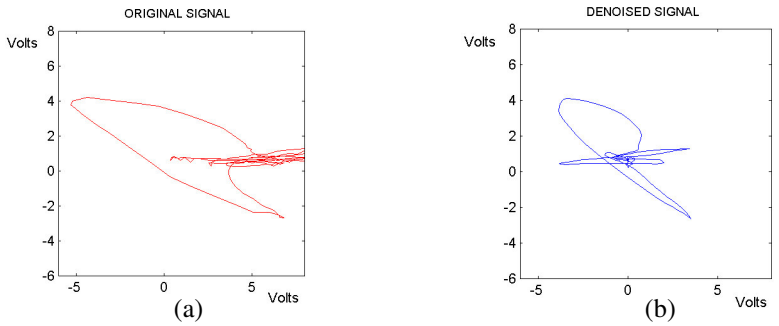

Figure 12. Original and denoised signal for ∅ 1,1 mm full depth hole

On the other hand, the phase angle of 41° is compatible to both Lissajous figures and the inductive voltage range of 6V is the expected value for a ∅ 1,1 mm defect. This problem can be solved by normalization of the signals using either the *RMS* value or the standard deviation value for the original signals, and it is the subject of an ongoing research.

5. Conclusions

The denoising of *ECT* signals through *MTN* removing using *WT* coefficients and *DEFECT CODES* generation is a promising technique. However it shall be determined the adequate set of *WT* coefficients for several different known defects. This set of *WT* coefficients will constitute a *DEFECT LIBRARY* for that tube standard specification. This library can be used as a standard calibration procedure for further testing of similar specification tubes. The method described above is presently applied manually but the use of artificial intelligence such as Fuzzy Logic to automatically perform the inspection is being developed and it will be presented in a future work.

Acknowledgement

The authors would like to thank Mr. Osvaldo P. Negrão Jr. (Interativa – Manutenção Preditiva Ltda.), for his help and assistance.

References

[1] Lopez, L. A. N. M., Wavelet Transform and Fuzzy Logic in the Eddy-Current Inspection of Nuclear Power Plants Steam Generator Tubes, PhD Thesis, IPEN, São Paulo, 2003.
[2] Lopez, L. A. N. M., Ting D. K. S., Upadhyaya, B. R., *Application of Wavelet Transform in De-Noising Eddy-Current Testing Signals of Heat Exchanger Tubes*. Proceedings of the 17th International Congress of Mechanical Engineering, São Paulo, SP, Brazil, 2003.
[3] Upadhyaya, B. R., Hooper, W., Yan, W., Behravesh, M. M., Henry, G. *Advances in Information Processing in Eddy-Current Diagnostics of Steam Generator Tubing,* Proceedings of the 9th Power Plant Dynamics, Control and Testing Symposium, 1995.
[4] Chen, G., Yamaguchi, A., Miya, K. *A Novel Signal Processing Technique for Eddy-Current Testing of Steam Generator Tubes*, IEEE Transactions on Magnetics, Vol. 34, N° 3, 1998.
[5] Stegemann, D. *Avanços Tecnológicos em END por Correntes Parasitas*, Revista dos END, pp. 23-29, 1986.
[6] Grman, J., Ravas, R., Syrová, L. *Application of Wavelet Transformation in Eddy Current Testing of Steam Generator Tubes*, Technology Conference, Budapest, Hungary: IEEE Instrumentation and Measurement, pp. 392-396, 2001.
[7] Li, L., Tsukda, K., Hanasaki, K., Liu, Z. *Fusion of Multi-Frequency Eddy Current Signals by Using Wavelet Analysis Method*, ISIF, pp. 108-113, 2002.
[8] Mallat, S. G. A Theory for Multiresolution Signal Decomposition: The Wavelet Representation, IEEE Trans. Pattern Anal. Mach. Intell. Vol. 11, pp. 674-693, July, 1989.
[9] Matlab, The Math Works Inc., Makron Books, 1997.